Supporting information

for

High entropy alloy nanoparticles encapsulated into carbon nanotubes enable high performance of zinc air battery

Shuyuan Pan[a,b#], Han Shi[b#], Yingjie Yu[a], Yifei Li[c], Yazhou Chen[a]*, Chunsheng Li[d,e], Yan Sun[d,e]*, Zehui Yang[b] and Fang Luo[a]*

[a]College of Materials Science and Engineering, State Key Laboratory of New Textile Materials & Advanced Processing Technology, Wuhan Textile University, Wuhan, 430200, China.

[b]Faculty of Materials Science and Chemistry, China University of Geosciences Wuhan, 388 Lumo RD, Wuhan, 430074, China.

[c]School of Engineering, Huzhou University, Huzhou, 313000, China

[d]School of Chemistry and Life Sciences, Suzhou University of Science and Technology, Suzhou City, Jiangsu Province 215009, China.

[e]Key Laboratory of Advanced Electrode Materials for Novel Solar Cells for Petroleum and Chemical Industry of China, Suzhou University of Science and Technology, Suzhou City, Jiangsu Province 215009, China.

Experimental section

Synthesis of FeCoNiMnIr/NCNT: Dicyandiamide (1.5 g, 99%, Sigma-Aldrich), $CoCl_2 \cdot 6H_2O$ (0.2 mmol, 97%, Sigma-Aldrich), $FeCl_3 \cdot 6H_2O$ (0.2 mmol, 98%, Sigma-Aldrich), $NiCl_2 \cdot 6H_2O$ (0.2 mmol, 98%, Sigma-Aldrich), $MnCl_2 \cdot 6H_2O$ (0.2 mmol, 99%, Sigma-Aldrich), $IrCl_3$ (0.1 mmol, 99.8%, Sigma-Aldrich) and 80 mL of ethanol were stirred and mixed for 2 h at room temperature (25 ^oC). Consequently, the mixture was heated to 80 ^oC and stirred to evaporate the solvent. The obtained powder was transferred to a mortar and ground into a fine powder. The powder was then placed in a tube furnace and heated under N_2 at 10 ^oC min^{-1} to 800 ^oC for 2 h to produce FeCoNiMnIr/NCNT electrocatalyst. Fe/NCNT was synthesized by heating $FeCl_3 \cdot 6H_2O$ and dicyandiamide at 800 ^oC for 2 h under N_2 flow. NCNT was obtained by strong acid (1 M H_2SO_4) treatment of Fe/NCNT at 60 ^oC for 10 h.

Fundamental characterizations: The phase analysis of the samples was obtained by XRD pattern obtained from Bruker D8 Advance. Structure characterization of the electrocatalyst was analyzed by X-ray photoelectron spectroscopy (XPS) (ThermoFisher, USA). The microscopic morphology of these samples was obtained by observation with a field emission electron microscope (SEM, SU8010, Japan). The microstructure and EDS mapping of the samples were analyzed by high resolution electron projection microscopy (TEM, FEI themis 300, United States).

Oxygen evolution reaction (OER): At room temperature, the three-electrode system (glassy carbon electrode-working electrode, carbon rod-counter electrode, Hg/HgO electrode-reference electrode) was used to complete the oxygen evolution reaction (OER) performance test by the Gamry Interface 1000E instrument. 2 mg of the

catalyst was dispersed into 1 mL solution, which was made up of 780 μL of deionized water, 200 μL of ethanol and 20 μL of Nafion. And the electrocatalyst loading on working electrode (a diameter of 3 mm) surface was 0.285 mg cm^{-2}. The performance test of the catalyst was measured by LSV (5 mV s^{-1}, 1.1-1.8 V vs. RHE), and the stability was measured by CA.

Oxygen reduction reaction (ORR): The ORR test environment was the same as the OER test. In a saturated O_2 environment, the three-electrode system was used to test the oxygen reduction performance of the catalyst, except that the working electrode was replaced with a rotating disk electrode (RDE). The configuration of "Ink" was the same as that of OER. The catalyst loading on the working electrode (a diameter of 4 mm) was 0.285 mg cm^{-2}. The performance test of the catalyst was measured by LSV (5 mV s^{-1}, 1.1-1.8 V vs. RHE) at different rotating speeds (400, 600, 800, 1200, 1600, 2400 rpm) and the stability was measured by i-t.

Aqueous zinc-air battery test: A home-made zinc air battery performance testing device was used. The active area was 1*1 cm and commercial zinc foil was polished before using as anode. PTFE plate was used to seal the electrolyte (6 M KOH+0.2 M zinc acetate). The electrocatalyst (1 mg) was dispersed in ethanol (200 μL), 5 wt% Nafion solution (20 μL) and deionized water (780 μL) by sonication. The resultant electrocatalyst ink was sprayed onto a 1*1 cm carbon paper. During the long-term operation, the electrolyte was manually replaced every 50 h.

All-solid-state zinc-air battery test: Polyvinyl alcohol (PVA, 1 g) was dissolved in 10 mL of deionized water to swell, and then heated to 95 ^{o}C until the polymer was

completely dissolved for 2 h, and then electrolyte (consisting of 18 M KOH+0.2 M zinc acetate，1 mL) was added dropwise , the obtained jelly was scraped (400 μm) with a spatula on a flat glass plate, frozen for 1 h, refrigerated for 12h, and immersed in the same electrolyte for 12 h before being used. The battery composition was basically the same as that of aqueous zinc-air battery, except that the electrolyte was replaced with a polymer electrolyte.

Table S1 Comparison of zinc air battery performance with recently reported electrocatalysts.

Electrocatalyst	Power density (mW cm^{-2})	Reference
FeCoNiMnIr/NCNT	214	This work
Fe_3C/Fe_2O_3@NGN	139.8	[1]
Co/CoO@FeNC-850	132.8	[2]
Co-NC@LDH	107.8	[3]
Co_3O_4@NiFe LDH	127.4	[4]
FeNiS-NBC/C	133.0	[5]
P-CoNi@NSCs	87.9	[6]
Ni–Co/NFC_{-2}	138.0	[7]
TMB@NiNC	107.0	[8]
Ni_3S_4@CoSx-NF	143.0	[9]
$Sr_2Fe_{1.5}Mo_{0.5}O_{6-\delta}$	137.0	[10]
MnOx-FeNi LDH/NF	120	[11]
Co-NC@Nb-TiOx	123.46	[12]

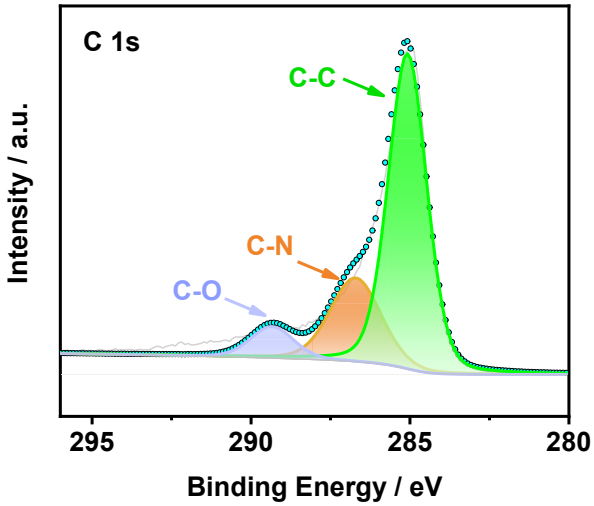

Figure S1 C 1s XPS peak of FeCoNiMnIr/NCNT.

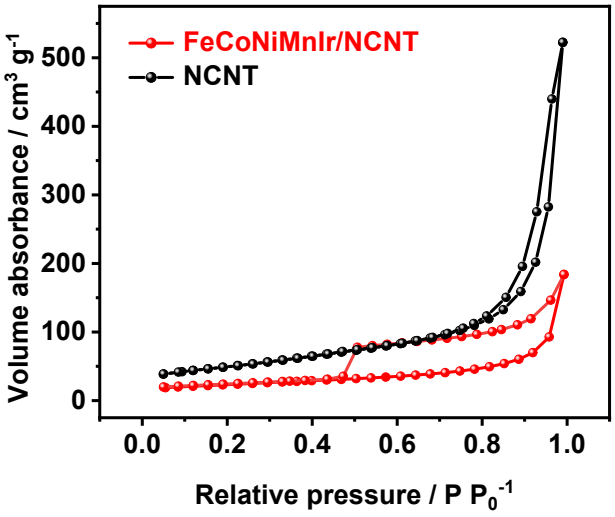

Figure S2 N_2 isothermal curves of NCNT and FeCoNiMnIr/NCNT.

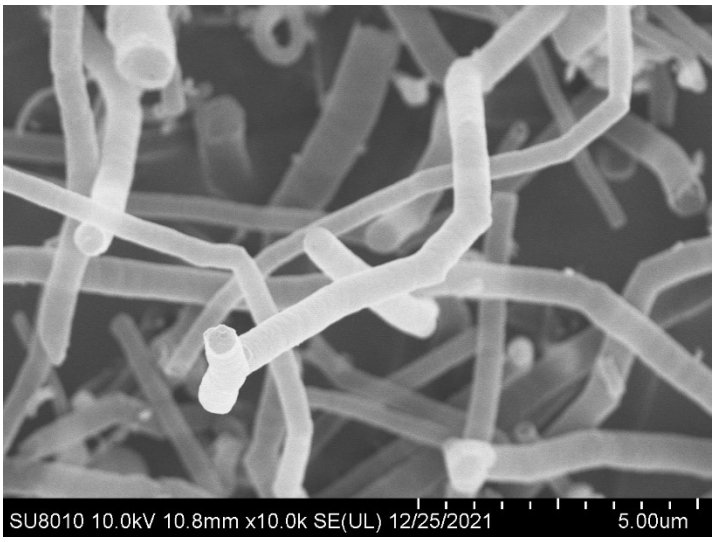

Figure S3 SEM image of NCNT.

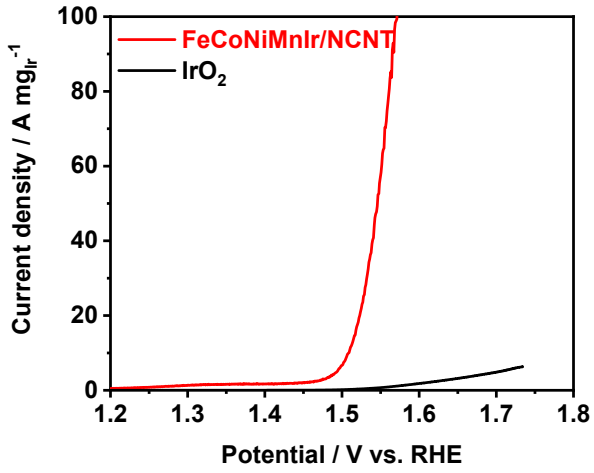

Figure S4 Mass activity of FeCoNiMnIr/NCNT and commercial IrO_2.

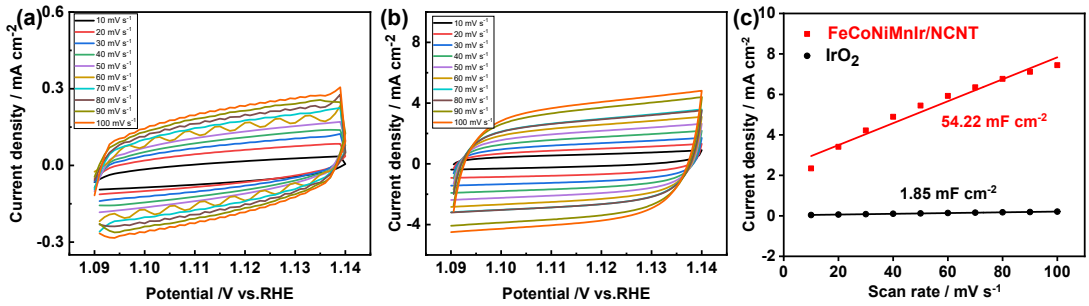

Figure S5 Cyclic voltammetry curves of IrO_2 (a) and FeCoNiMnIr/NCNT (b). C_{dl} of IrO_2 and FeCoNiMnIr/NCNT.

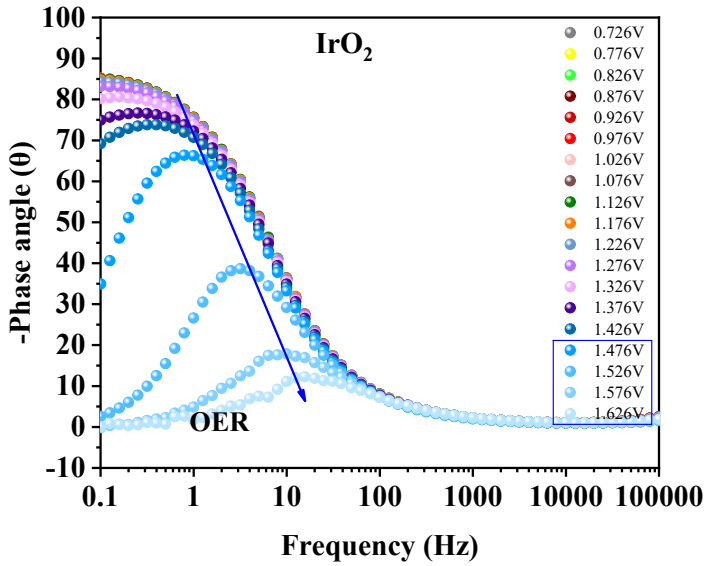

Figure S6 *in-situ* electrochemical impedance spectroscopy of commercial IrO_2.

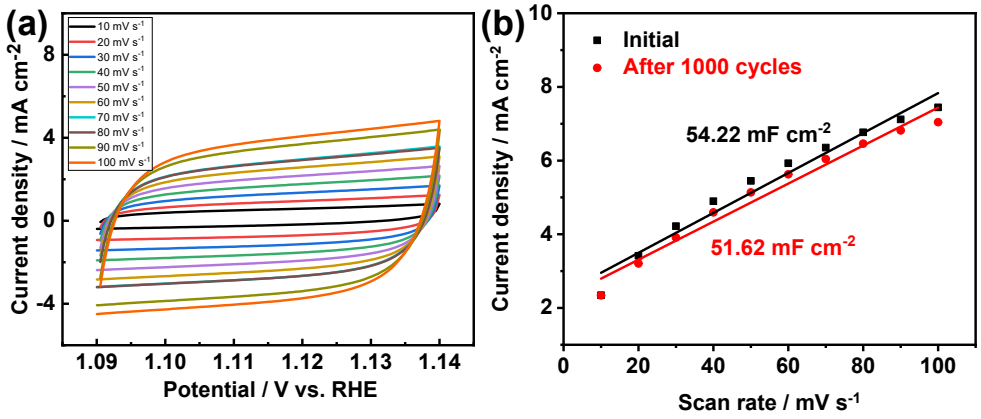

Figure S7 Cyclic voltammetry curve (a) and C_{dl} (b) of FeCoNiMnIr/NCNT after 1000 cycles.

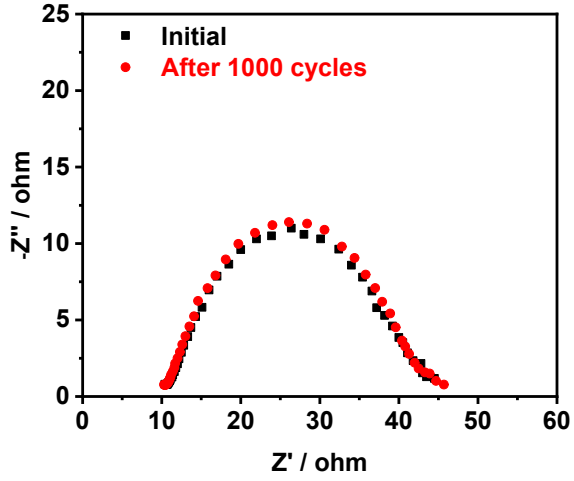

Figure S8 Electrochemical impedance spectroscopy of FeCoNiMnIr/NCNT before and after 1000 cycles.

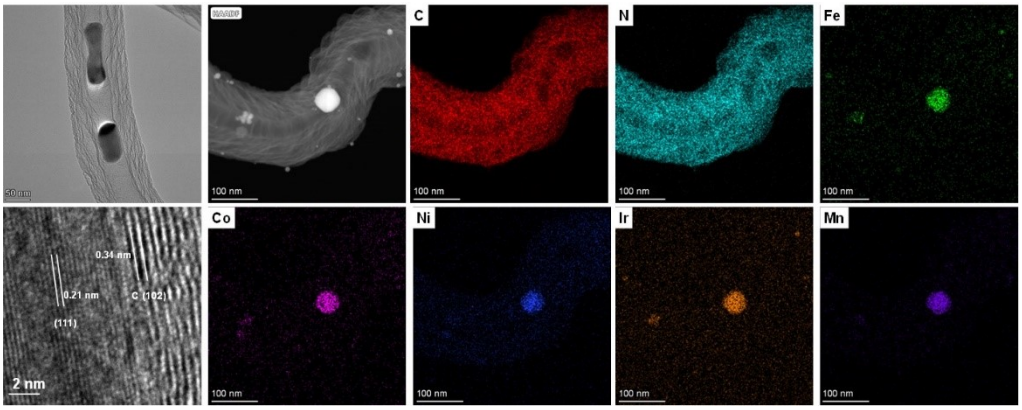

Figure S9 TEM, HR-TEM, HAADF-STEM and relative EDS mapping of FeCoNiMnIr/NCNT after 1000 cycles.

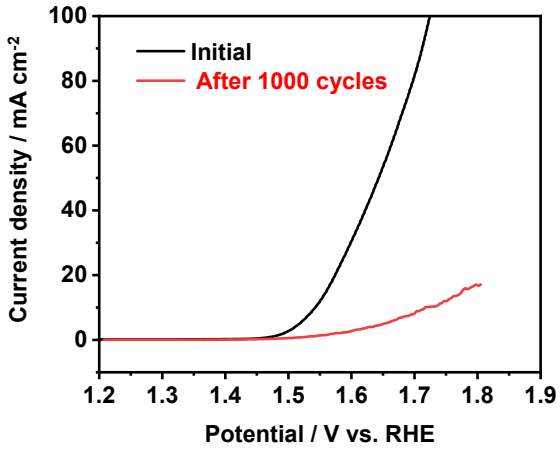

Figure S10 OER performance of commercial IrO_2 before and after 1000 cycles.

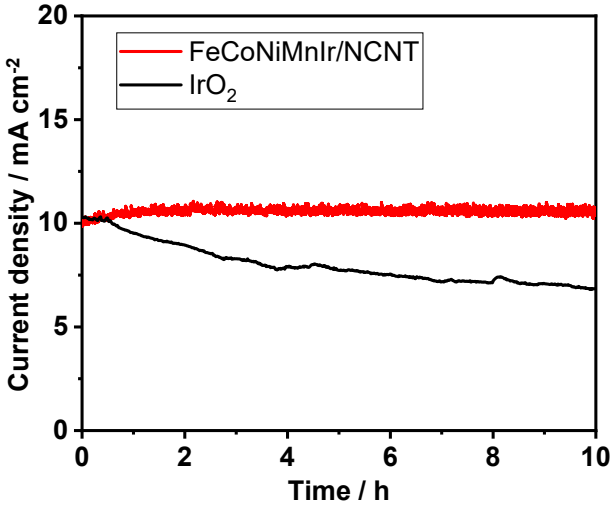

Figure S11 i-t test of FeCoNiMnIr/NCNT and commercial IrO_2.

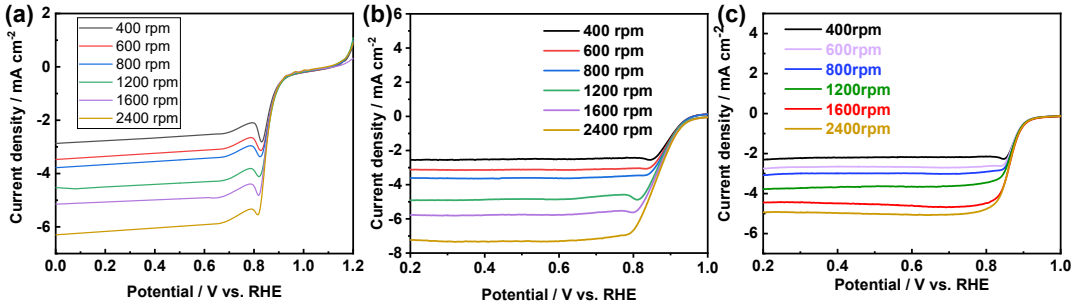

Figure S12 ORR curves of commercial Pt/C (a), FeCoNiMnIr/NCNT (b) and NCNT (c).

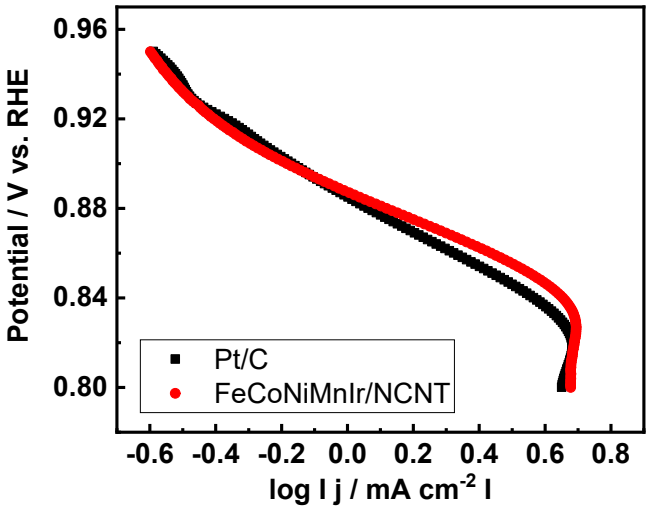

Figure S13 Tafel slope of FeCoNiMnIr/NCNT and Pt/C.

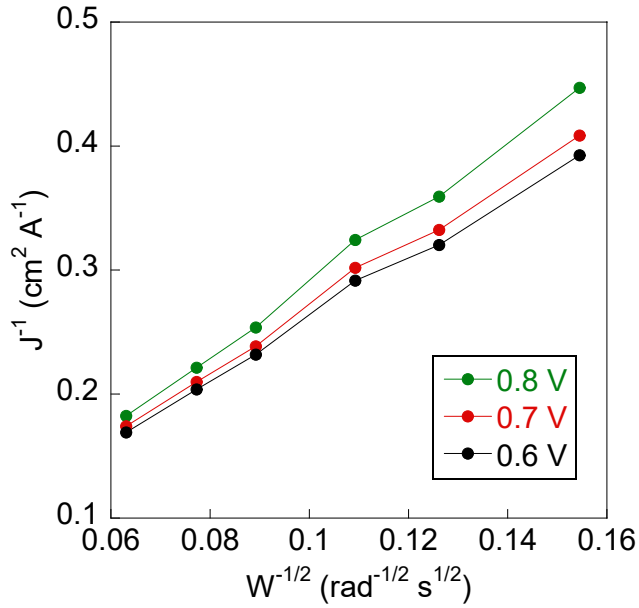

Figure S14 K-L equation of commercial Pt/C at various potentials.

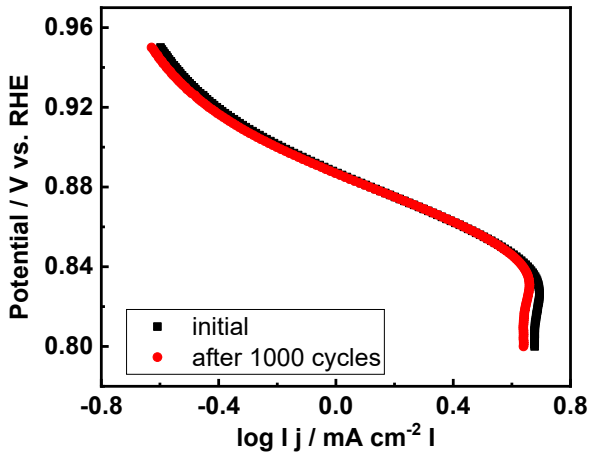

Figure S15 Tafel slope of FeCoNiMnIr/NCNT before and after 1000 cycles.

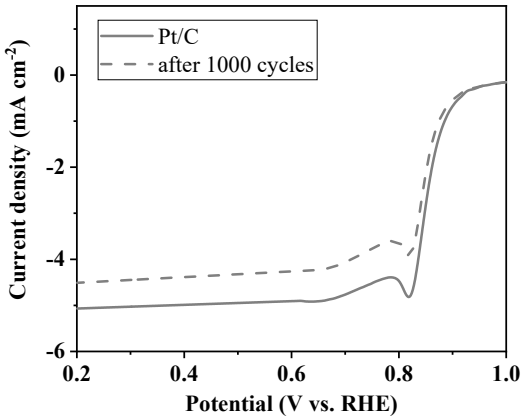

Figure S16 ORR stability test of commercial Pt/C.

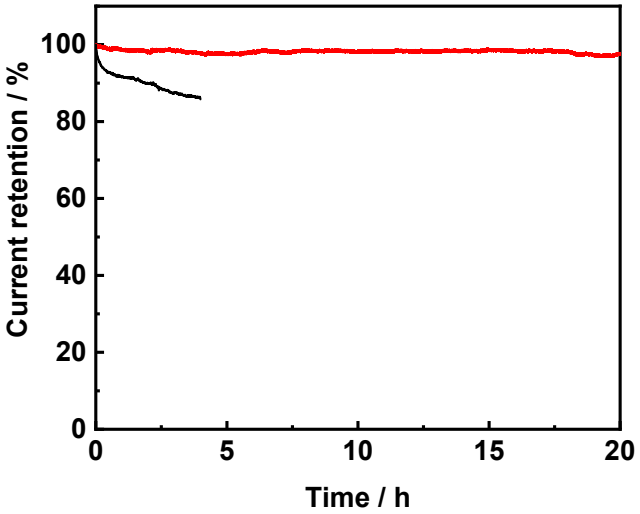

Figure S17 i-t test of Pt/C and FeCoNiMnIr/NCNT in ORR catalysis.

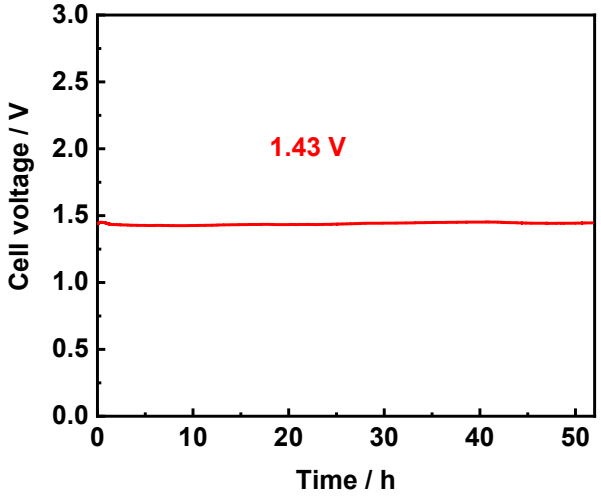

Figure S18 Open circuit voltage test of rechargeable zinc air battery assembled from FeCoNiMnIr/NCNT.

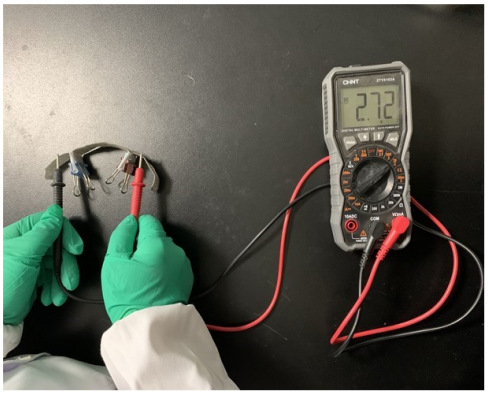

Figure S19 Open circuit voltage test of two all-solid-state rechargeable zinc air batteries.

References

1. Y. H. Tian, L. Xu, J. C. Qian, J. Bao, C. Yan, H. N. Li, H. M. Li and S. Q. Zhang, *Carbon*, 2019, **146**, 763-771.
2. Y. Chen, C. Gong, Z. Shi, D. Chen, X. Chen, Q. Zhang, B. Pang, J. Feng, L. Yu and L. Dong, *Journal of Colloid and Interface Science*, 2021, **596**, 206-214.
3. D. Chen, X. Chen, Z. Cui, G. Li, B. Han, Q. Zhang, J. Sui, H. Dong, J. Yu, L. Yu and L. Dong, *Chemical Engineering Journal*, 2020, **399**.
4. X. L. Guo, X. L. Hu, D. Wu, C. Jing, W. Liu, Z. L. Ren, Q. N. Zhao, X. P. Jiang, C. H. Xu, Y. X. Zhang and N. Hu, *Acs Applied Materials & Interfaces*, 2019, **11**, 21506-21514.
5. Y. X. Wang, R. J. Liu, W. D. Chen, W. M. Li, W. Zheng, H. Zhang and Z. Y. Zhang, *Acs Sustainable Chemistry & Engineering*, 2022, **10**, 14486-14494.
6. X. H. He, J. Fu, M. Y. Niu, P. F. Liu, Q. Zhang, Z. Y. Bai and L. Yang, *Electrochimica Acta*, 2022, **413**.
7. M. H. Wang, S. Ji, H. Wang, V. Linkov, X. Y. Wang and R. F. Wang, *Journal of Power Sources*, 2023, **571**.
8. M. Moloudi, A. Noori, M. S. Rahmanifar, Y. Shabangoli, M. F. El-Kady, N. B. Mohamed, R. B. Kaner and M. F. Mousavi, *Advanced Energy Materials*, 2022, DOI: 10.1002/aenm.202203002.
9. M. M. Yin, H. Miao, J. X. Dang, B. Chen, J. Q. Zou, G. M. Chen and H. Li, *Journal of Power Sources*, 2022, **545**.
10. J. Zhou, T. Liu, J. Zhang, L. Zhao, W. He and Y. Wang, *Separation and Purification Technology*, 2023, **304**.
11. L. Wan, P. C. Wang, Y. Q. Lin and B. G. Wang, *Journal of the Electrochemical Society*, 2019, **166**, A3409-A3415.
12. T. T. Wan, H. Y. Wang, L. L. Wu, C. C. Wu, Z. S. Zhang, S. M. Liu, J. Fu and J. D. Li, *Journal of Colloid and Interface Science*, 2023, **651**, 27-35.